Journal of Magnetism and Magnetic Materials 485 (2019) 8–15

Contents lists available at ScienceDirect

Journal of Magnetism and Magnetic Materials

journal homepage: www.elsevier.com/locate/jmmm

Research articles

Comparative study on the forming and reversion of strain-induced martensite in two duplex stainless steels: Developing a model for VSM analysis of powders or fine chips

D.J.M. de Aguiar[a,*], A.F. Padilha[b], R.L. Plaut[b], M.R. da Silva[c], N.B. de Lima[d]

[a] Departamento Acadêmico de Mecânica, DAMEC, Universidade Tecnológica Federal do Paraná – UTFPR, Avenida Monteiro Lobato, s/n – Km 04, Ponta Grossa, PR, Brazil

[b] Departamento de Engenharia Metalúrgica e de Materiais, Escola Politécnica da Universidade de São Paulo, EPUSP, Av. Professor Mello Moraes, 2463 – Butantã, São Paulo, SP, Brazil

[c] Instituto de Física e Química, Universidade Federal de Itajubá – UNIFEI, Av. B P S, 1003 – Pinheirinho, Itajubá, MG, Brazil

[d] Centro de Ciência e de Tecnologia em Materiais, CCTM, Instituto de Pesquisas Energéticas e Nucleares – IPEN, Av. Prof. Lineu Prestes, 2242 São Paulo, SP, Brazil

ARTICLE INFO

Keywords:
Duplex stainless steels
Fit equation
Magnetic saturation
Strain-induced martensite (α′)
X-ray diffraction

ABSTRACT

An original feature of this work is the proposal of two equations to fit the volume fraction of ferromagnetic (α + α′) phases that can be applied in the measurement of magnetic saturation of comminuted duplex and superduplex stainless steels (for example, powders or filed chips). Duplex stainless steels contain similar volume fractions of austenite (γ) and ferrite (α) in their microstructure. Two steels exemplify this class, namely the most widely used duplex UNS S31803 and superduplex UNS S32520 stainless steels. The phenomena of work hardening, formation, and reversion of strain-induced martensite (α′) in austenite were compared in both stainless steels. Samples were work-hardened and annealed under identical conditions, and their behavior was evaluated mainly through X-ray diffraction and magnetic measurements. Notably, the volume fraction of strain-induced α′ in duplex stainless steel was as high as 32%, which indicated that this steel had a greater tendency to form α′ than superduplex stainless steel, for which the corresponding value equaled 15%. Annealing at 650 °C for 2 h promoted the reversion of strain-induced α′ into γ, decreasing the volume fraction of the former phase from 32 to 2% (duplex) and from 15 to 6% (superduplex).

1. Introduction

Wrought duplex stainless steels (DSS) present equivalent volume fractions of ferrite (α) and austenite (γ) in their microstructure lamellae or alternate plates. The presence of α and γ in the microstructure of the DSS assures that this class of steels has an attractive combination of properties. In a DSS, the yield strength is practically twice the yield strength of the typical ferritic and austenitic stainless steels. Another favorable characteristic of the DSS is its excellent corrosion resistance because of the presence of chromium, molybdenum, and nitrogen in high concentrations. Steels having a duplex microstructure exhibit a favorable combination of mechanical strength and chemical resistance, finding varying applications mainly geared toward chemically aggressive environments [1–3]. Both α and γ phases of DSS exhibit characteristics and behaviors that are quite different from each other during straining. The body-centered cubic (BCC) α has high stacking-fault energy (SFE) and is not susceptible to strain-induced phase transformations, thereby exhibiting a much lower strain hardening exponent. The face-centered cubic γ, with a lower SFE than α, is susceptible to strain-induced phase transformations and exhibits higher strain hardening during cold work. For example, the SFE of austenitic stainless steels types AISI 304L and 316L is in the order of 15–18 and 25–64 mJ/m^2, respectively [4–13]. In these austenitic stainless steels, particularly in AISI 304L, there is a significant formation of strain-induced martensite (SIM-α′).

SIM-α′ is a very fine phase that can be visualized by optical or scanning electron microscopy [14–16]. However, finer details are difficult to detect without the use of larger magnifications, and hence, the use of transmission electron microscopy is necessitated [17]. On the other hand, the BCC lattice of SIM-α′ is identical to that of α, and both SIM-α′ and α are ferromagnetic. Therefore, the SIM-α′ of austenitic stainless steels is easily detected and quantified by X-ray diffraction

* Corresponding author.
E-mail addresses: denilsonaguiar@utfpr.edu.br (D.J.M. de Aguiar), padilha@usp.br (A.F. Padilha), rlplaut@usp.br (R.L. Plaut), mrsilva@unifei.edu.br (M.R. da Silva), nblima@ipen.br (N.B. de Lima).

https://doi.org/10.1016/j.jmmm.2019.04.054
Received 9 August 2018; Received in revised form 13 April 2019; Accepted 14 April 2019
Available online 15 April 2019
0304-8853/ © 2019 Elsevier B.V. All rights reserved.

(XRD) because several peaks appear with same the lattice parameters of α during straining; however, these peaks are absent prior to work hardening. Therefore, it is possible to perform phase quantification by considering the relative areas measured under the peaks [18]. In the case of the DSS, the detection and quantification of SIM-α′ is relatively difficult because of the presence of α. Still, the direct comparison method provides high accuracy, because changes in the intensity of peaks due to phase formation during work hardening and reversion during heat treatment can be compared. Thus, the differences in the peak intensity from strained to the heat-treated material can be attributed to the presence of SIM-α′. An alternative approach to detect SIM-α′ is through magnetic measurements, as the presence of SIM-α′ increases magnetic saturation once the material is exposed to an external applied field, as in the case of vibrating sample magnetometry (VSM) [19–23].

The transformation of γ into SIM-α′ has been extensively studied in both the austenitic stainless steels and in the DSS grades. For example, some studies have described the transformation of γ into SIM-α′ as function of thickness reduction by cold rolling degrees in DSS [20,23–26]. In addition, in a lean DSS, which has low nitrogen content—and therefore, a highly metastable austenite—the complete transformation of austenite into SIM-α′ has already been reported [23]. In other works, the behavior can be described as an exponential function [20] or a sigmoidal function [24], having transformation saturation close to 30%; alternatively, the behavior can be described as polynomial with lower saturation of transformation, close to 10% [25,26].

The reversion of SIM-α into γ has also been the subject of several studies since the 1990s [27,28] and has continued to be a topic of interest [29–35]. For example, in lean DSS type, reversion was still associated as an important parameter on the material's grain refinement [36]. However, there is insufficient data and understanding on SIM-α′ formation and its reversion in DSS. Therefore, the present work attempts to study the partial transformation of γ into SIM-α′ by means of XRD and magnetic saturation measurements for two DSS. In addition, this work also attempts to study the reversion of SIM-α′ into γ caused by annealing.

2. Materials

The chemical compositions of UNS S31803 DSS and UNS S32520 superduplex (SDSS) steels utilized in this study are listed in Table 1.

2.1. Preliminary characterization

The samples were received in the solution-annealed condition, which were initially characterized using optical microscopy techniques, quantitative stereology (measurement of volume fraction and grain size), scanning electron microscopy, and energy dispersive spectroscopy. The samples were polished and etched using the Beraha solution (20 mL HCl, 80 mL H_2O and 0.3 g of potassium metabisulfite), which were used in the stereological evaluations conducted using optical microscopy. In addition, thermal etching using a liquefied petroleum gas (LPG) flame for 1 min was used to enhance the phase contrast.

Table 1
Chemical composition (mass%) of the two types of duplex stainless steel used in this work (balance is Fe).

UNS S31803 (DSS)									
C	Si	Mn	P	S	Cr	Ni	Mo	Cu	N
0.0234	0.278	1.797	0.0374	0.0010	22.52	5.54	3.246	0.148	0.157
UNS S32520 (SDSS)									
C	Si	Mn	P	S	Cr	Ni	Mo	Cu	N
0.0236	0.295	0.867	0.0464	0.0004	24.90	6.50	4.044	1.399	0.218

2.2. Stacking fault energy (SFE)

The SFE evaluation, which is based on the chemical composition of the steel, can be performed using several equations reported in literature [4,37–39]. It is worth pointing out that most of these equations were developed to evaluate austenitic stainless steels and hence the results of SFE evaluation for DSS austenites may be inaccurate [26]. Among them, some SFEs (mJ/m^2) are given by:

$$\text{Schramm and Reed}\,[4, 37] = -53 + 6.2(\%Ni) + 0.7(\%Cr) + 3.2(\%Mn) + 9.3(\%Mo) \quad (1)$$

$$\text{Rhodes and Thompson}\,[37, 38] = 1.2 + 1.4(\%Ni) + 0.6(\%Cr) + 17.7(\%Mn) - 44.7(\%Si) \quad (2)$$

$$\text{Pickering}\,[37, 39] = 25.7 + 2(\%Ni) + 410(\%C) - 0.9(\%Cr) - 77(\%N) - 13(\%Si) - 1.2(\%Mn) \quad (3)$$

2.3. Straining, annealing, and characterization of particles

After initial characterization, each steel sample was filed to obtain fine chips. Filing was done carefully to avoid heating [4]. It should be noted that comminution via filing has three objectives—to minimize the strong crystallographic texture normally present in the DSS [21,36,40], to introduce a large number of crystalline defects through random distribution of chips during XRD measurements (and considering them as a powder), and to obtain the SIM-α′ [4,41–46]. In addition, a complementary analysis of particle size and particle size distribution was performed by using Malvern Mastersizer 2000.

After hand filing, a fraction of the chips was encapsulated under vacuum and annealed for 2 h in order to evaluate the SIM-α′ reversion. Two temperatures were used, namely 600 and 650 °C, based on the temperature range recommended in literature [27,28,31,47]. The difference between the values of stereology and XRD—which is discussed in the next section—for the α volume fraction can be attributed to SIM-α′ formation during filing [4]. Thus, the effects of annealing could also be evaluated. Therefore, the following equation can be used to evaluate the total volume fraction of martensite (α′) in the material:

$$\alpha' = \text{Total of BCC}\,(\alpha + \alpha'\ \text{by XRD}) - \text{initial ferrite}\,(\alpha\ \text{by stereology}) \quad (4)$$

The related sample treatment conditions are listed in Table 2.

2.4. XRD analysis

The characterization of the work hardened and annealed chips was performed mainly by using XRD, in a Rigaku diffractometer using Cu radiation (λ = 0.15408 nm). The fine chips filed were considered as a powder (random distribution), without strong crystallographic texture. This allowed us to carry out precise measurements of quantitative analyses by using XRD. It is important to emphasize that α and SIM-α′ have the same lattice parameters; therefore, both phases diffract X-rays in the same position. This implies that the peak area obtained is a sum of both contributions. The volume fraction of γ and α plus SIM-α′

Table 2
Conditions used to treat DSS (A) and SDSS (B) samples.

Condition	Samples	
	A (duplex DSS)	B (superduplex SDSS)
Work hardened	A1	B1
Annealed 600 °C/2 h	A2	B2
Annealed 650 °C/2 h	A3	B3

(α + α′) phases can be calculated using the following equations [18]:

$$I_\alpha/I_\gamma = R_\alpha c_\alpha/R_\gamma c_\gamma, \quad (5)$$

$$R_{\alpha,\gamma} = 1/v^2[|F|^2 m(1 + \cos^2\theta/\sin^2\theta\cos\theta)](e^{-2M}/2\mu), \quad (6)$$

$$C_\alpha + C_\lambda = 1. \quad (7)$$

The volume fraction and additional parameters of γ and α plus SIM-α′ (α + α′) phases was determined by the Rietveld method based on the above considerations. Rietveld refinement was performed using GSAS software [48] by inputting the adequate phase crystallographic information files (cif), instrumental parameters, and diffraction data. The "goodness of fit" (GoF) or Chi-square (χ^2) of the parameter values was followed by graphical comparison, which is a valid and recognized refinement criterion [48,49]. The χ^2 GoF parameter was calculated using the following equation:

$$\chi^2 = [R_{wp}/R_{exp}]^2, \quad (8)$$

where R_{wp} is related to the observed intensity in diffractogram, and R_{exp} is related to the expected intensity calculated from the pattern [18,48,49]. The refinement was considered good when χ^2 attained values as close as possible to unity [48,49].

2.5. VSM measurements

A complementary magnetic saturation experiment was performed using a VSM machine (Lake Shore, model 7400 VSM) [20,21,50], to estimate the volume fraction of the ferromagnetic (α + α′) phases. Eq. (9) was used for DSS [20,21,50] and Eq. (10) was used for SDSS [51]:

$$C(\alpha)\% = M\_s/133, \quad (9)$$

$$C(\alpha)\% = M\_s/128, \quad (10)$$

where *M_s* (emu/g) is the outcome of magnetic saturation measurement (emu/g), and values of 133 and 128 emu/g are the intrinsic magnetic saturations of DSS [20,21,50] and SDSS [51], respectively.

2.6. Equations for analysis of fine chips by VSM measurements

The volume fractions measured by XRD were assumed to be the most accurate measurements for the chip condition. Thus, for each steel, it was possible to organize the values obtained by XRD on the *y*-axis and the values calculated from the magnetic saturation measurements on the *x*-axis. For this method, a pair of values was taken for each steel and arranged in ascending order of *y*. Further, the results were extrapolated, 100% was adopted as a point of convergence among the techniques.

Subsequently, two new equations were developed to replace equations (9) and (10) in the analysis of fine chips by VSM in duplex and superduplex stainless steels, respectively.

3. Results and discussion

3.1. Preliminary results

The microstructures of the as-received materials in the solution annealed condition were identical and represented lamellae or alternate plates of α and γ, with elongated grains originated from processing. This morphology is typical of rolled DSS sheets and can be justified by the lower interfacial energy (γ/α) when compared to the grain boundary energies of (α/α) and (γ/γ). Fig. 1 shows 3D optical micrograph image the UNS S31803 DSS, where the sample was etched by heating using an LPG flame (about 1 min. on each face).

The quantities of both phases (α and γ) in the sheet (in the initial solution annealed condition) were assessed. Both phases in the sheet were evaluated using the grid method according to the ASTM E 562 [52] along the three surfaces: longitudinal, transversal, and on the rolling surface. The XRD method was discarded because of the strong crystallographic texture of the sheets [21,40]. Moreover, the grain size was assessed according to the ASTM E 112 [53] standard. These procedures were performed for both steels (DSS and SDSS). The stereology measurements of as-received UNS S31803 DSS gave a 44 ± 4% ferrite volume fraction and a grain size of 25 μm of ferrite and austenite. In the UNS S32520 SDSS, the ferrite volume fraction was 45 ± 4% and grain sizes of ferrite and austenite were 35 and 34 μm, respectively. The partition of elements was assessed for both phases of the two stainless steels by using energy dispersive spectroscopy (EDS), as listed in Table 3. As expected, α was richer in chrome and molybdenum, whereas γ had higher nickel content. Partition coefficients observed in this work were in reasonable agreement with those in the literature [24].

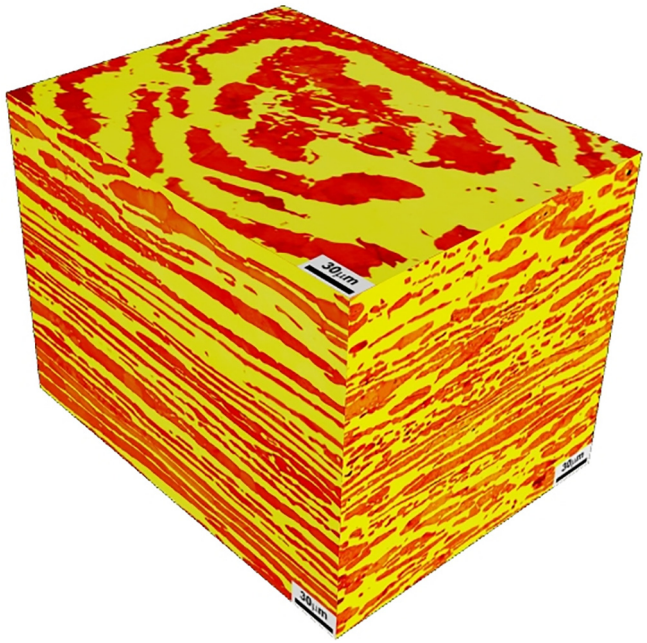

Fig. 1. Optical microscopy composition along three dimensions of the UNS S31803 duplex stainless steel.

3.2. SFE values from literature equations

Table 4 lists the SFE values, which were derived based on equations (1)–(3) and taking into account the global chemical composition and austenite chemical composition of duplex and superduplex steels estimated by EDS analysis.

The SFE calculated using equations (1)–(3) diverged greatly from each other. For example, Schramm's and Rhodes' equations resulted in very high values of SFE for both steels and appear to be unrealistic, as already reported before [26]. Pickering's equation results in values of

Table 3
Mass contents (%) of the elements in α and γ, partitioning of the elements in the two phases (α/γ), determined through energy dispersive analysis of the DSS and SDSS.

Element	Duplex (DSS) Mass (%)			Superduplex (SDSS) Mass (%)			Partition α/γ obtained from Ref. [24]
	α	γ	α/γ	α	γ	α/γ	
Fe	66.59	68.97	0.97	63.16	64.27	0.98	0.97
Cr	23.68	21.7	1.09	27.3	24.44	1.12	1.17
Ni	4.44	6.93	0.64	5.31	8.39	0.63	0.61
Mo	3.6	2.44	1.48	4.22	2.91	1.45	1.59

Table 4
SFE values calculated from different equations present in literature, by using global composition and austenite composition for both steels.

Method (equation)	Material			
	Duplex Global composition	SFE (mJ/m^2) Austenite composition	Superduplex Global composition	SFE (mJ/m^2) Austenite composition
Schramm and Reed [4,37]	33	41	45	55
Rhodes and Thompson [37,38]	42	57	27	43
Pickering [37,39]	8	19	4	19

8–19 and 4–19 mJ/m^2 for DSS and SDSS, respectively. These ranges of values were generated by an approach similar to that used for calculating the SFE, namely by using the global composition of steels or the composition of austenite estimated by EDS. In both cases, the values seem plausible, and do not differ significantly from those determined by TEM (10 mJ/m^2) [24]. Even though the equations have been developed for austenitic stainless steels, the Pickering equation seems provide reasonable values for duplex grade steels, and appears to be more realistic than the values obtained using other equations.

It is reported in literature that SFE is a very important parameter in the determining the mechanism of plastic deformation. This parameter can be restrictive in the martensitic transformation. The value of 18 mJ/m^2 is reported as limit for the martensitic transformation; below this limit, the transformation occurs and above it, transformation does not occur. As the values estimated in the present work are in agreement with this value, the martensitic transformation is expected to occur in both steels [54].

3.3. Considerations for hand filing straining and particle size results

Manual filing has been reported as capable of introducing high levels of crystalline defects in several materials [4,41–46] as well as producing large amounts of SIM-α′ in a single step [4]. However, as regards the degree of deformation, it is still regarded as an undefined control method. Despite of this challenge, the saturation values on the formation of the SIM-α′ found in this work were in agreement with the results of other published works. Fig. 2, illustrates an adaptation by plotting the values found in this work and from the literature [20,24–26]. As the deformation degree of the filing is undefined, the *x*-axis of the graph was marked with "??".

A summary of the particle size and size distribution of the filing chips for DSS and SDSS are listed in Table 5. Particle size distribution was performed using Malvern Mastersizer 2000.

From Table 5, for D10, we can see that 10% of particles are below 69 µm for duplex and 76 µm for superduplex. Similar reasoning can be followed for D50 and D90, giving values of size distribution. The average particles size of duplex stainless steel filing chips is 198 µm

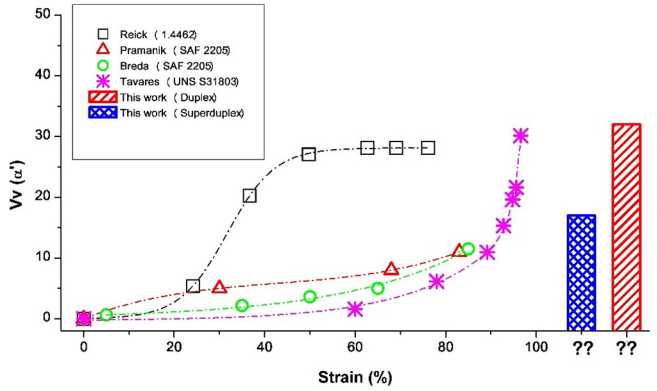

Fig. 2. Adaptation of SIM-α′ vs. % straining by cold rolling from literature [20,24–26] and results obtained in present work by filing.

Table 5
Particle size and size distribution for DSS and SDSS.

Material	D10 (µm)	D50 (µm)	D90 (µm)	Average size (µm)
Duplex	69	169	374	198
Superduplex	76	190	410	219

while that for the superduplex is 219 µm. In practice, the filing chips for both steels have very close average and distribution sizes.

3.4. Effects of straining and annealing on the X-ray diffraction results

Fig. 3A and B show the effects of work hardening via hand filing and subsequent annealing for DSS and SDSS, respectively, in terms of the XRD results. The conditions of each sample are listed in Table 2, and they are marked on the diffractogram. Lines of α and γ phase diffraction are also marked on the figure.

For both steels in the work hardened condition, the peaks of the BCC (α + SIM-α′) phases have higher relative intensity than those in the annealed condition at 600 and 650 °C. This intensity increase corresponds to the formation of SIM-α′.

The quantitative analysis, which was performed using Rietveld refinement on the GSAS software [48], takes into account the relative height and width of the peaks [18]. The volume fraction of BCC (α + SIM-α′) and lattice parameters of the phases are listed in Table 6. The formed and reversed quantities were assessed according to equation (4), taking into account the XRD results and the presence of α in the initial material, as observed through stereology.

The reversion of the SIM-α′ phase into γ due to annealing performed at 600 and 650 °C for 2 h in both steels can be observed clearly. Taking into account the calculated values through the quantitative stereology as the reference, both steels presented an incomplete reversion, leaving behind a residual fraction of 2% of SIM-α′ for DSS and 6% of SIM-α′ for SDSS.

Summarizing the results, the amount of BCC phase observed in SDSS chips obtained through hand filing was smaller than that in DSS. This may be attributed to the smaller amount of interstitial nitrogen present in the DSS (strong austenite stabilizer), which renders the austenite of these steels more metastable [55–60]. The same effect is observed with DSS, which has low nitrogen content, and its austenite is highly metastable and can be fully transformed into SIM-α′ during straining [23].

3.5. Magnetic measurements results

Fig. 4A (UNS S31803 DSS) and 4B (UNS S32520 SDSS) show the magnetic saturation tests, which were conducted on the as-received, work-hardened, and annealed steels for 2 h at 600 and 650 °C.

The magnetic saturation values and the amount of ferromagnetic BCC (α + α′) phases were calculated using equation (9) and (10), for duplex and superduplex steel, respectively. As described in Table 7, the quantification of ferromagnetic (α + α′) phases for both steels performed by magnetic saturation method was compared with those obtained by stereology for the as-received material and XRD method for the filed chips. It was observed that the BCC phase values obtained

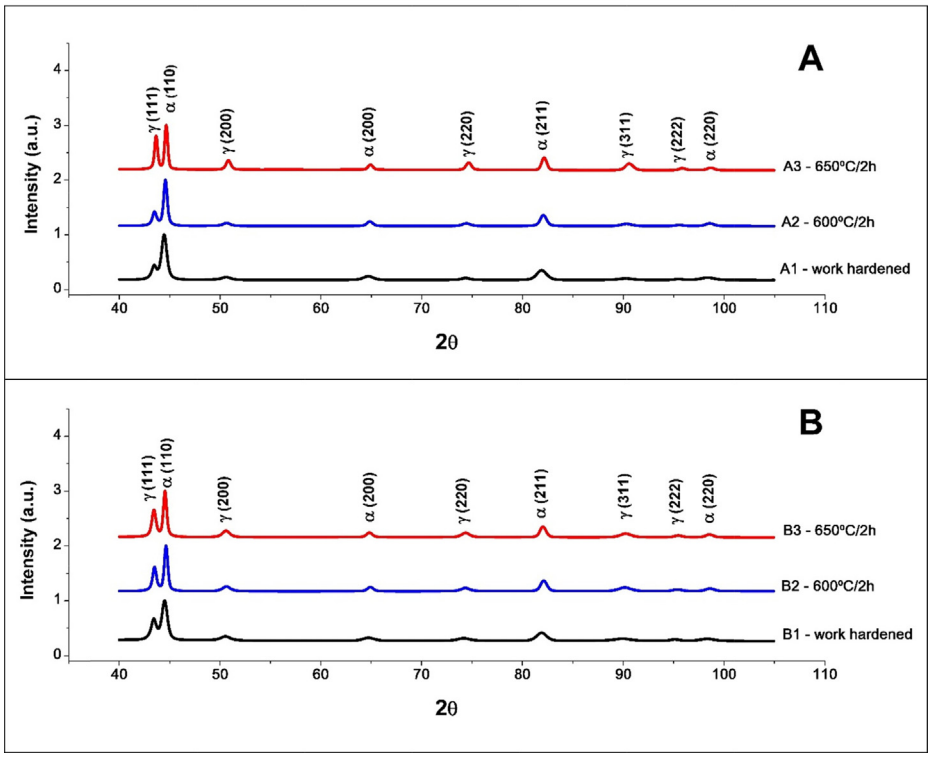

Fig. 3. X-ray diffraction patterns of chips produced by hand filing, work hardened, and annealing for (A) duplex UNS S31803 and (B) superduplex UNS S32520. Radiation: Cu K_{α}.

Table 6
Lattice parameters of the phases and volume fractions after refinement. The goodness of fit (χ^2) parameter is listed for each sample.

Sample	Parameters						GoF
	lattice γ (nm)	lattice α (nm)	Total Vv α (%)	Total Vv γ (%)	Initial α (%)	SIM-α′ (%)	χ2
A1	0.361	0.288	76	24	44	32	1.15
A2	0.361	0.288	69	31	44	25	1.50
A3	0.360	0.288	46	54	44	2	1.37
B1	0.362	0.288	60	40	45	15	1.11
B2	0.362	0.288	56	44	45	11	1.16
B3	0.361	0.288	51	49	45	6	1.19

using the VSM values for the initial sheet are in agreement with quantitative stereology measurements for both steels. The volume fraction values of magnetic phase (α + α′) from filed and heat-treated chips showed apparently systematic discrepancies between the XRD and magnetic saturation methods for both steels.

The magnetic saturation tests resulted in smaller magnetic phase fraction (α + α′) than the fractions calculated using the XRD analyses. Some studies have shown that powdered materials have lower magnetic saturation than bulk materials. This is because with decreasing particle size, the surface to volume ratio increases, resulting in lower magnetic saturation [61,62]. Although these reports suggest a different class of materials, apparently, filed chips were affected by the same phenomena; hence, the quantification may be underestimated.

Although the values obtained using the two methods do not match exactly, it is possible to observe a consistent correlation between the two methods.

3.6. Equations to fit the magnetic saturation method for comminuted duplex and superduplex stainless steels

Fig. 5A (for duplex) and B (for superduplex) show two graphs, which are obtained by plotting the values listed in Table 7. As mentioned earlier, the volume fraction obtained by magnetic saturation can be underestimated because of particle size [61,62]. Moreover, a

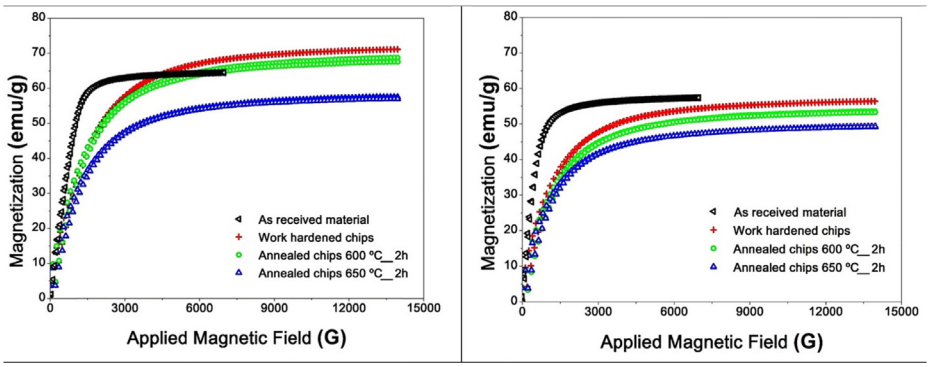

Fig. 4. Results of magnetic measurements for (A) UNS S31803 DSS and (B) UNS S32520 SDSS chips obtained through filing and annealed at 600 and 650 °C for 2 h.

Table 7
Fraction volume of ferromagnetic (α + α′) phases using VSM values, calculated using equations (9) and (10) for duplex and superduplex steels, respectively.

Condition	Material					
	Duplex			Superduplex		
	M_s (emu/g)	*Cα*(%) by magnetic saturation method	*Cα*(%) by stereology (as received) and XRD (filed chips)	*M_s* (emu/g)	*Cα*(%) by magnetic saturation method	*Cα*(%) by stereology (as received) and XRD (filed chips)
As received	64.2	48	44	58.2	46	45
Work hardened	74.9	56	76	58.7	46	60
600 °C/2 h	72.3	54	69	56.0	44	56
650 °C/2 h	60.5	46	46	51.4	40	51

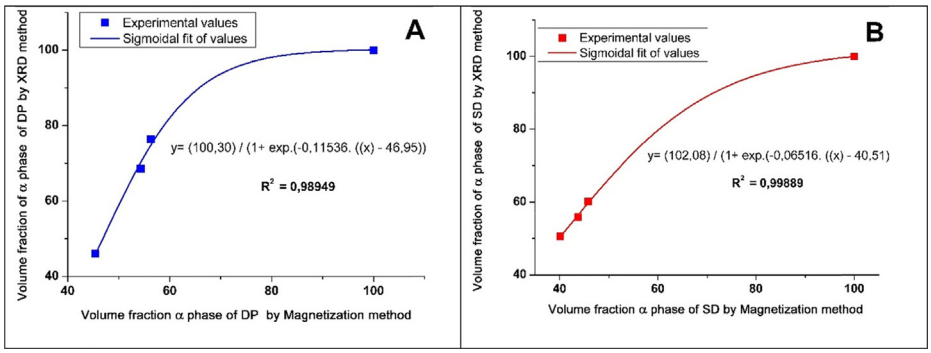

Fig. 5. Volume fraction of (α + α′) phase calculated from magnetic saturation values vs. volume fraction of (α + α′) phase calculated from XRD. A represents duplex stainless steel and B represents superduplex stainless steel.

Table 8
Volume fraction (α + α′) of phases measured by XRD and fitted by equation (11) and (12) for duplex and superduplex stainless steel, respectively (VSM %).

Condition	Material					
	Duplex			Superduplex		
	(%) XRD	(%)VSM	error (%)	(%) XRD	(%)VSM	error (%)
Work hardened	76	75	+1.3	60	60	0.0
600 °C/2h	69	70	−1.4	56	56	0.0
650 °C/2h	46	46	0.0	51	50	+2.0

sigmoidal correlation was observed between both methods for each steel. Moreover, it was possible to fit the magnetic saturation measurements by adapting some equations in literature, to be used for comminuted DSS [20,21,50] (equation (11)), and for SDSS [51] (equation (12)), by the corrections given below:

$$C\_\alpha\, corr\,(\%) = (102.30)/((1 + \exp((-0.11536) \times ((100 \times (M\_s/M\_si)) - 46.95)), \quad (11)$$

$$C\_\alpha\, corr\,(\%) = (102.08)/((1 + \exp((-0.06516) \times ((100 \times (M\_s/M\_si)) - 40.51)), \quad (12)$$

where *M_s* is the outcome of a magnetic saturation measurement (emu/g), and *M_si* is the intrinsic magnetic saturation of a given material (emu/g; 133 emu/g for DSS [20,21,50] and 128 emu/g for SDSS [51]). The volume fraction of ferromagnetic BCC (α + α′) phases of filed DSS and SDSS chips, and their fitted values obtained using correction given by equations (11) and (12), respectively, are listed in Table 8.

Eq. (11) was verified using the magnetic saturation values of DSS powders available in literature [19,50] and was found to be consistent, as evidenced in Supplementary material 1.

The values of the magnetic saturation measurement method, fitted by equations (11) and (12) to estimate ferromagnetic (α + α′) phase volume fraction, are closer to XRD values and do not deviate by more than 2%. A phase transformation may be detected via the annealing of the strained chip because of a decrease in the magnetic saturation values [20–23,50]. This decrease can be attributed to the SIM-α′ reversion in austenite; this observed decrease is higher for the heat treatment for 2 h at 650 °C than for 600 °C in both cases.

4. Conclusions

In this work, we undertook a comparative study on the forming and reversion of strain-induced martensite in two duplex stainless steels, which led to the development of two fit equations. It was realized that one of them should be used for DSS and the other for SDSS. These equations were developed to fit the values of the magnetic saturation method, by taking into account the measurements of the filed chips/powder (comminuted DSS grades). Through X-ray and magnetic saturation measurements, it was observed that the hand filing method led to the transformation of austenite into strain-induced martensite in both steels. However, the studied duplex stainless steel presented a higher strain induced martensite fraction than the superduplex stainless steel (32.4% vs. 15.2%). It was possible to study the reversion of strain-induced martensite into austenite in duplex stainless steels by Rietveld refinement of X-ray diffraction data and also by VSM. The quantitative results from X-ray diffraction and from the fit equation of VSM data are in reasonable agreement with each other, with a difference of no more than 2%.

Conflicts of interest

The authors have no conflicts of interest to declare.

Acknowledgments

Authors would like to thank CNPq (Conselho Nacional de Desenvolvimento Científico e Tecnológico) for financial support and Professor Marcelo de Aquino Martorano (EPUSP) and Professor Eduardo Franco de Monlevade (EPUSP) for assisting in the revision of the manuscript.

Appendix A. Supplementary data

Supplementary data to this article can be found online at https://doi.org/10.1016/j.jmmm.2019.04.054.

References

[1] I. Alvarez-Armas, Duplex stainless steels: brief history and some recent alloys, Recent Pat. Mech. Eng. 1 (2008) 51–57, https://doi.org/10.2174/2212797610801010051.
[2] I.A. Ward, L.H. Keys, Application of stress corrosion cracking theory to duplex stainless steels, in: Institute of Metals Book, Stainless Steels 84, Institute of Metals, Gothenburg, 1985, pp. 373–376.
[3] K. Fukaura, H. Izumi, H. Kawabe, Tensile properties of microduplex stainless steel at low temperature, J. Soc. Mater. Sci., Jpn. 35 (1986) 603–609, https://doi.org/10.2472/jsms.35.603.
[4] R.E. Schramm, R.P. Reed, Stacking fault energies of seven commercial austenitic stainless steels, Metall. Trans. A 6 (1975) 1345–1351, https://doi.org/10.1007/BF02641927.
[5] S. Catalao, X. Feaugas, P. Pilvin, M.T. Cabrillat, Dipole heights in cyclically deformed polycrystalline AISI 316L stainless steel, Mater. Sci. Eng., A 400–401 (2005) 349–352, https://doi.org/10.1016/j.msea.2005.03.094.
[6] S.G. Chowdhury, S. Das, P.K. De, Cold rolling behaviour and textural evolution in AISI 316L austenitic stainless steel, Acta Mater. 53 (2005) 3951–3959, https://doi.org/10.1016/j.actamat.2005.05.006.
[7] X. Feaugas, C. Gaudin, Ratchetting process in the stainless steel AISI 316L at 300 K: an experimental investigation, Int. J. Plast. 20 (2004) 643–662, https://doi.org/10.1016/S0749-6419(03)00076-7.
[8] F. Forouzan, A. Najafizadeh, A. Kermanpur, A. Hedayati, R. Surkialiabad, Production of nano/submicron grained AISI 304L stainless steel through the martensite reversion process, Mater. Sci. Eng., A 527 (2010) 7334–7339, https://doi.org/10.1016/j.msea.2010.08.002.
[9] C. Gaudin, X. Feaugas, Cyclic creep process in AISI 316L stainless steel in terms of dislocation patterns and internal stresses, Acta Mater. 52 (2004) 3097–3110, https://doi.org/10.1016/j.actamat.2004.03.011.
[10] B. Ravi Kumar, B. Mahato, N.R. Bandyopadhyay, D.K. Bhattacharya, Comparison of rolling texture in low and medium stacking fault energy austenitic stainless steels, Mater. Sci. Eng., A 394 (2005) 296–301, https://doi.org/10.1016/j.msea.2004.11.057.
[11] S. Mishra, K. Narasimhan, I. Samajdar, Deformation twinning in AISI 316L austenitic stainless steel: role of strain and strain path, Mater. Sci. Technol. 23 (2007) 1118–1126, https://doi.org/10.1179/174328407X213242.
[12] J. Talonen, H. Hänninen, Formation of shear bands and strain-induced martensite during plastic deformation of metastable austenitic stainless steels, Acta Mater. 55 (2007) 6108–6118, https://doi.org/10.1016/j.actamat.2007.07.015.
[13] D.N. Wasnik, I.K. Gopalakrishnan, J.V. Yakhmi, V. Kain, I. Samajdar, Cold rolled texture and microstructure in types 304 and 316L austenitic stainless steels, ISIJ Int. 43 (2003) 1581–1589, https://doi.org/10.2355/isijinternational.43.1581.
[14] S. Papula, S. Anttila, J. Talonen, T. Sarikka, I. Virkkunen, H. Hänninen, Strain hardening of cold-rolled lean-alloyed metastable ferritic-austenitic stainless steels, Mater. Sci. Eng., A 677 (2016) 11–19, https://doi.org/10.1016/j.msea.2016.09.038.
[15] J. Talonen, P. Aspegren, H. Hänninen, Comparison of different methods for measuring strain induced α-martensite content in austenitic steels, Mater. Sci. Technol. 20 (2004) 1506–1512, https://doi.org/10.1179/026708304X4367.
[16] A. Hedayati, A. Najafizadeh, A. Kermanpur, F. Forouzan, The effect of cold rolling regime on microstructure and mechanical properties of AISI 304L stainless steel, J. Mater. Process. Technol. 210 (2010) 1017–1022, https://doi.org/10.1016/j.jmatprotec.2010.02.010.
[17] M.C. Young, S.L.I. Chan, L.W. Tsay, C.-S. Shin, Hydrogen-enhanced cracking of 2205 duplex stainless steel welds, Mater. Chem. Phys. 91 (2005) 21–27, https://doi.org/10.1016/j.matchemphys.2004.10.042.
[18] B.D. Cullity, Elements of X-ray Diffraction, second ed., Addison-Wesley Publishing Company Inc., Lebanon, Indiana, 1978.
[19] C.S.P. Mendonça, A.N.O. Dias, M.L.N.M. Melo, V.A.S. Ribeiro, M.R. da Silva, A.F. Oliveira, G. Silva, Evaluation of high-energy milling efficiency in stainless steel with addition of vanadium carbides, Int. J. Adv. Manuf. Technol. 95 (2018) 3093–3099, https://doi.org/10.1007/s00170-017-1297-7.
[20] S.S.M. Tavares, M.R. da Silva, J.M. Pardal, H.F.G. Abreu, A.M. Gomes, Microstructural changes produced by plastic deformation in the UNS S31803 duplex stainless steel, J. Mater. Process. Technol. 180 (2006) 318–322, https://doi.org/10.1016/j.jmatprotec.2006.07.008.
[21] M.A. Ribeiro Miranda, J.M. Sasaki, S.S.M. Tavares, H.F.G. de Abreu, J.M. Neto, The use of X-ray diffraction, microscopy, and magnetic measurements for analysing microstructural features of a duplex stainless steel, Mater. Charact. 54 (2005) 387–393, https://doi.org/10.1016/j.matchar.2004.12.009.
[22] K.H. Lo, J.K.L. Lai, On the cryogenic magnetic transition and martensitic transformation of the austenite phase of 7MoPLUS duplex stainless steel, J. Magn. Magn. Mater. 322 (2010) 2335–2339, https://doi.org/10.1016/j.jmmm.2010.02.034.
[23] S. Baldo, I. Mészáros, Effect of cold rolling on microstructure and magnetic properties in a metastable lean duplex stainless steel, J. Mater. Sci. 45 (2010) 5339–5346, https://doi.org/10.1007/s10853-010-4582-5.
[24] W. Reick, M. Pohl, A.F. Padilha, Determination of stacking fault energy of austenite in a duplex stainless steel, Steel Res. Int. 67 (1996) 253–256, https://doi.org/10.1002/srin.199605486.
[25] S. Pramanik, S. Bera, S.K. Ghosh, Influence of cold rolling on microstructural evolution in 2205 duplex stainless steel, Steel Res. Int. 85 (2014) 776–783, https://doi.org/10.1002/srin.201300293.
[26] M. Breda, K. Brunelli, F. Grazzi, A. Scherillo, I. Calliari, Effects of cold rolling and strain-induced martensite formation in a SAF 2205 duplex stainless steel, Metall. Mater. Trans. A 46 (2015) 577–586, https://doi.org/10.1007/s11661-014-2646-x.
[27] K. Tomimura, S. Takaki, S. Tanimoto, Y. Tokunaga, Chemical composition in Fe-Cr-Ni alloys for ultra grain refining by reversion from deformation induced martensite, ISIJ Int. 31 (1991) 721–727, https://doi.org/10.2355/isijinternational.31.721.
[28] K. Tomimura, S. Takaki, Y. Tokunaga, Reversion mechanism from deformation induced martensite to austenite in metastable austenitic stainless steels, ISIJ Int. 31 (1991) 1431–1437, https://doi.org/10.2355/isijinternational.31.1431.
[29] Y. Yagodzinskyy, J. Pimenoff, O. Tarasenko, J. Romu, P. Nenonen, H. Hänninen, Grain refinement processes for superplastic forming of AISI 304 and 304L austenitic stainless steels, Mater. Sci. Technol. 20 (2004) 925–929, https://doi.org/10.1179/026708304225019678.
[30] T. Tsuchiyama, Y. Nakamura, H. Hidaka, S. Takaki, Effect of initial microstructure on superplasticity in ultrafine grained 18Cr-9Ni stainless steel, Mater. Trans. 45 (2004) 2259–2263, https://doi.org/10.2320/matertrans.45.2259.
[31] E. Dryzek, M. Sarnek, M. Wróbel, Reverse transformation of deformation-induced martensite in austenitic stainless steel studied by positron annihilation, J. Mater. Sci. 49 (2014) 8449–8458, https://doi.org/10.1007/s10853-014-8555-y.
[32] H.Y. Yi, F.K. Yan, N.R. Tao, K. Lu, Comparison of strength–ductility combinations between nanotwinned austenite and martensite–austenite stainless steels, Mater. Sci. Eng., A 647 (2015) 152–156, https://doi.org/10.1016/j.msea.2015.08.065.
[33] A. Kisko, J. Talonen, D.A. Porter, L.P. Karjalainen, Effect of Nb microalloying on reversion and grain growth in a high-Mn 204Cu austenitic stainless steel, ISIJ Int. 55 (2015) 2217–2224, https://doi.org/10.2355/isijinternational.ISIJINT-2015-156.
[34] A. Kisko, A.S. Hamada, J. Talonen, D. Porter, L.P. Karjalainen, Effects of reversion and recrystallization on microstructure and mechanical properties of Nb-alloyed low-Ni high-Mn austenitic stainless steels, Mater. Sci. Eng., A 657 (2016) 359–370, https://doi.org/10.1016/j.msea.2016.01.093.
[35] N. Gong, H. Wu, G. Niu, J. Cao, D. Zhang, Tana, Effect of martensitic transformation on nano/ultrafine-grained structure in 304 austenitic stainless steel, J. Iron Steel Res. Int. 24 (2017) 1231–1237, https://doi.org/10.1016/S1006-706X(18)30022-0.
[36] A. Mandal, S. Patra, D. Chakrabarti, S.B. Singh, Effect of rolling and subsequent annealing on microstructure, microtexture, and properties of an experimental duplex stainless steel, Metall. Mater. Trans. A 48 (2017) 5960–5977, https://doi.org/10.1007/s11661-017-4345-x.
[37] K.H. Lo, C.H. Shek, J.K.L. Lai, Recent developments in stainless steels, Mater. Sci. Eng., R 65 (2009) 39–104, https://doi.org/10.1016/j.mser.2009.03.001.
[38] C.G. Rhodes, A.W. Thompson, The composition dependence of stacking fault energy in austenitic stainless steels, Metall. Trans. A 8 (1977) 1901–1906, https://doi.org/10.1007/BF02646563.
[39] F.B. Pickering, Physical metallurgical development of stainless steels, in: Institute of Metals Book, Stainless Steels 84, Institute of Metals, Gothenburg, 1985, pp. 2–28.
[40] M. ElMassalami, I. Palatnik-de-Sousa, M.C.L. Areiza, J.M.A. Rebello, A. Elzubair, On the magnetic anisotropy of superduplex stainless steel, J. Magn. Magn. Mater. 323 (2011) 2403–2407, https://doi.org/10.1016/j.jmmm.2011.05.007.
[41] B.E. Warren, X-ray studies of deformed metals, Prog. Met. Phys. 8 (1959) 147–202, https://doi.org/10.1016/0502-8205(59)90015-2.
[42] D.E. Mikkola, J.B. Cohen, Effects of thermal-mechanical treatments on faulting in some fcc alloys, J. Appl. Phys. 33 (1962) 892–898, https://doi.org/10.1063/1.1777187.
[43] E.N. Aqua, C.N.J. Wagner, X-ray diffraction study of deformation by filing in B.C.C. refractory metals, Philos. Mag. 9 (1964) 565–589, https://doi.org/10.1080/14786436408211871.
[44] C.L. Corey, D.I. Potter, Recovery processes and ordering in Ni_3Al, J. Appl. Phys. 38 (1967) 3894–3900, https://doi.org/10.1063/1.1709036.
[45] F.W. Arnoth, J.P. Clark, G.P. Mohanty, A diffraction study of the substructure in cold-worked Ni_3Al, J. Appl. Phys. 48 (1977) 1771–1777, https://doi.org/10.1063/1.323926.
[46] M. Khitouni, A.W. Kolsi, N. Njah, X-ray investigation of mechanical milling of Ni_3Al (0.2wt% B) powder: disordering, crystallite refinement and microstrains, Phys. Chem. News 9 (2003) 131–136.
[47] A.D.I. Schino, I. Salvatori, J.M. Kenny, Effects of martensite formation and austenite reversion on grain refining of AISI 304 stainless steel, J. Mater. Sci. 37 (2002) 4561–4565, https://doi.org/10.1023/A:1020631912685.

[48] A.C. Larson, R.B. Von Dreele, General structure analysis system (GSAS), Los Alamos National Laboratory Report LAUR 86-748 (2004), Los Alamos, 2004. https://subversion.xray.aps.anl.gov/trac/EXPGUI (accessed 13 April 2019).
[49] B.H. Toby, R factors in Rietveld analysis: how good is good enough? Powder Diffr. 21 (2006) 67–70, https://doi.org/10.1154/1.2179804.
[50] C. de S.P. Mendonça, A.F. Oliveira, L.A. Oliveira, M.R. da Silva, M. de L.N.M. Melo, G. Silva, Structural and magnetic properties of duplex stainless steel (UNS S31803) powders obtained by high energy milling of chips with additions of NbC, Mater. Res. 21 (2017) e20170717, https://doi.org/10.1590/1980-5373-mr-2017-0717.
[51] S.S.M. Tavares, J.M. Pardal, J.A. de Souza, J.M. Neto, M.R. da Silva, Magnetic phase quantification of the UNS S32750 superduplex stainless steel, J. Alloys Compd. 416 (2006) 179–182, https://doi.org/10.1016/j.jallcom.2005.09.006.
[52] ASTM E562-11, Standard test method for determining volume fraction by systematic manual point count, ASTM Int. (2011) 1–7, https://doi.org/10.1520/E0562-11.
[53] ASTM Standard E112-13, Standard test methods for determining average grain size, ASTM Int. (2014) 1–28, https://doi.org/10.1520/E0112-13.
[54] S. Allain, J.P. Chateau, O. Bouaziz, S. Migot, N. Guelton, Correlations between the calculated stacking fault energy and the plasticity mechanisms in Fe-Mn-C alloys, Mater. Sci. Eng., A 387–389 (2004) 158–162, https://doi.org/10.1016/j.msea.2004.01.059.
[55] P. Rozenak, Effects of nitrogen on hydrogen embrittlement in AlSl type 316, 321 and 347 austenitic stainless steels, J. Mater. Sci. 25 (1990) 2532–2538, https://doi.org/10.1007/BF00638055.
[56] M. Sumita, T. Hanawa, S.H. Teoh, Development of nitrogen-containing nickel-free austenitic stainless steels for metallic biomaterials—review, Mater. Sci. Eng., C 24 (2004) 753–760, https://doi.org/10.1016/j.msec.2004.08.030.
[57] J.Y. Choi, J.H. Ji, S.W. Hwang, K.-T. Park, Effects of nitrogen content on TRIP of Fe–20Cr–5Mn–xN duplex stainless steel, Mater. Sci. Eng., A 534 (2012) 673–680, https://doi.org/10.1016/j.msea.2011.12.025.
[58] M. Talha, C.K. Behera, O.P. Sinha, A review on nickel-free nitrogen containing austenitic stainless steels for biomedical applications, Mater. Sci. Eng., C 33 (2013) 3563–3575, https://doi.org/10.1016/j.msec.2013.06.002.
[59] R.P. Reed, Nitrogen in austenitic stainless steels, JOM 41 (1989) 16–21, https://doi.org/10.1007/BF03220991.
[60] T.-H. Lee, C.-S. Oh, S.-J. Kim, Effects of nitrogen on deformation-induced martensitic transformation in metastable austenitic Fe–18Cr–10Mn–N steels, Scr. Mater. 58 (2008) 110–113, https://doi.org/10.1016/j.scriptamat.2007.09.029.
[61] G. Campillo, A. Gil, O. Arnache, J.J. Beltrán, J. Osorio, G. Sierra, Analysis of magnetic and structural properties in $La_{0.6}Sr_{0.4}MnO_3$ ferromagnetic particles under the influence of mechanical ball milling effect, J. Phys.: Conf. Ser. 466 (2013) 012022, https://doi.org/10.1088/1742-6596/466/1/012022.
[62] X. He, W. Zhong, C.-T. Au, Y. Du, Size dependence of the magnetic properties of Ni nanoparticles prepared by thermal decomposition method, Nanoscale Res. Lett. 8 (2013) 446, https://doi.org/10.1186/1556-276X-8-446.